Decadal acidification in the water masses of the Atlantic Ocean

Aida F. Ríos[a,1], Laure Resplandy[b], Maribel I. García-Ibáñez[a], Noelia M. Fajar[a], Anton Velo[a], Xose A. Padin[a], Rik Wanninkhof[c], Reiner Steinfeldt[d], Gabriel Rosón[e], and Fiz F. Pérez[a]

[a]Marine Research Institute, Spanish National Research Council (IIM-CSIC), E-36208 Vigo, Spain; [b]Scripps Institution of Oceanography, University of California, San Diego, La Jolla, CA 92037; [c]Atlantic Oceanographic and Meteorological Laboratory, National Oceanographic and Atmospheric Administration, Miami, FL 33149; [d]Oceanography Department, Institute of Environmental Physics, University of Bremen, 28359 Bremen, Germany; and [e]Faculty of Marine Sciences, University of Vigo, Campus Lagoas-Marcosende, E-36200 Vigo, Spain

Edited by François M. M. Morel, Princeton University, Princeton, NJ, and approved July 1, 2015 (received for review March 16, 2015)

Global ocean acidification is caused primarily by the ocean's uptake of CO_2 as a consequence of increasing atmospheric CO_2 levels. We present observations of the oceanic decrease in pH at the basin scale (50°S–36°N) for the Atlantic Ocean over two decades (1993–2013). Changes in pH associated with the uptake of anthropogenic CO_2 (ΔpHCant) and with variations caused by biological activity and ocean circulation (ΔpHNat) are evaluated for different water masses. Output from an Institut Pierre Simon Laplace climate model is used to place the results into a longer-term perspective and to elucidate the mechanisms responsible for pH change. The largest decreases in pH (ΔpH) were observed in central, mode, and intermediate waters, with a maximum ΔpH value in South Atlantic Central Waters of -0.042 ± 0.003. The ΔpH trended toward zero in deep and bottom waters. Observations and model results show that pH changes generally are dominated by the anthropogenic component, which accounts for rates between −0.0015 and −0.0020/y in the central waters. The anthropogenic and natural components are of the same order of magnitude and reinforce one another in mode and intermediate waters over the time period. Large negative ΔpHNat values observed in mode and intermediate waters are driven primarily by changes in CO_2 content and are consistent with (*i*) a poleward shift of the formation region during the positive phase of the Southern Annular Mode in the South Atlantic and (*ii*) an increase in the rate of the water mass formation in the North Atlantic.

ocean acidification | pH | anthropogenic carbon | water masses | climate model

The uptake of anthropogenic CO_2 (Cant) by the ocean has lowered seawater pH since preindustrial times. This large-scale and long-term change is referred to as "ocean acidification," a process that has led to changes in seawater carbonate chemistry (1–3) with impacts on the chemical speciation of seawater and biogeochemical cycles. A predominant effect is the decrease of carbonate ions in seawater that impacts calcareous marine organisms (4–6). The uptake of Cant is the main cause for the gradual reduction of seawater pH, but biological, physical, and chemical "natural" changes in the ocean, such as changes in the oxidation of organic matter, impact pH as well (7, 8).

Several studies have focused on ocean acidification in the last decade. Model-based studies have examined pH changes on a global scale (2, 9), and observation-based studies have focused on time-series stations (10–13) and specific regions such as the North Pacific (7, 14) and North Atlantic (8). However, investigations of basin-wide pH changes throughout the water column from direct measurements are sparse (15), in large part because of a dearth of quality referenced pH measurements.

In this study, we present the first (to our knowledge) measurement-based changes in pH along meridional lines in the Atlantic from 50°S–36°N using observations from three cruises: OACES/CO_2 (1993), CITHER-II (1994), and FICARAM-XV (2013) (Fig. 1*A* and *SI Appendix*, Table S1). We investigate the total change in pH and refer to it as acidification. The change in pH is separated into anthropogenic (ΔpHCant) and natural (ΔpHNat) components and is evaluated for the water masses along the section over two decades (1993–2013). Both components are related to Cant uptake and to processes such as the remineralization of organic matter and changes in water mass. The observed pH changes are compared with outputs from an Institut Pierre Simon Laplace (IPSL) climate model to place the observations into context and to elucidate the mechanisms controlling anthropogenic and natural pH changes, which are clearly discerned in climate models.

Results

More than 4,000 pH measurements referenced to the seawater scale (SWS) at 25 °C in the Atlantic Ocean (50°S–36°N) were examined to estimate the changes in oceanic pH between 1993 and 2013. We used pH measurements referenced to the SWS at 25 °C throughout this discussion, because the thermodynamic temperature effect over pH did not affect the interpretation of the results. Changes in pH were evaluated for the major water masses identified along the section based on their hydrographic properties (16). We differentiated five water masses in the North Atlantic following Talley et al. (17) and six water masses in the South Atlantic following Mémery et al. (18). Potential density (σ_θ, σ_3, σ_4) intervals were used as a reference (Fig. 1 and *SI Appendix*, Table S2). Furthermore, we divided the study area into three regions: southern (50°S–14°S), equatorial (14°S–18°N), and northern (18°N–36°N) (Fig. 1).

The overall patterns in pH distribution along this section in the Atlantic were similar in 1993–94 and 2013 (Fig. 2*A* and

Significance

We provide the first (to our knowledge) observation-based acidification trends in the water masses of the Atlantic basin over the past two decades and compare them with climate model results. Observations and model output confirm that pH changes in surface layers are dominated by the anthropogenic component. In mode and intermediate waters, the anthropogenic and natural components are of the same order of magnitude and sign. Large changes in the natural component of newly formed mode and intermediate waters are associated with latitudinal shifts of these water masses caused by the Southern Annular Mode in the South Atlantic and by changes in the rates of water mass formation in the North Atlantic.

Author contributions: A.F.R., L.R., and F.F.P. designed research; A.F.R., L.R., M.I.G.-I., R.W., R.S., G.R., and F.F.P. performed research; A.F.R., L.R., M.I.G.-I., N.M.F., A.V., X.A.P., R.W., R.S., G.R., and F.F.P. analyzed data; and A.F.R., L.R., and M.I.G.-I. wrote the paper.

The authors declare no conflict of interest.

This article is a PNAS Direct Submission.

Freely available online through the PNAS open access option.

[1]To whom correspondence should be addressed. Email: aida@iim.csic.es.

This article contains supporting information online at www.pnas.org/lookup/suppl/doi:10.1073/pnas.1504613112/-/DCSupplemental.

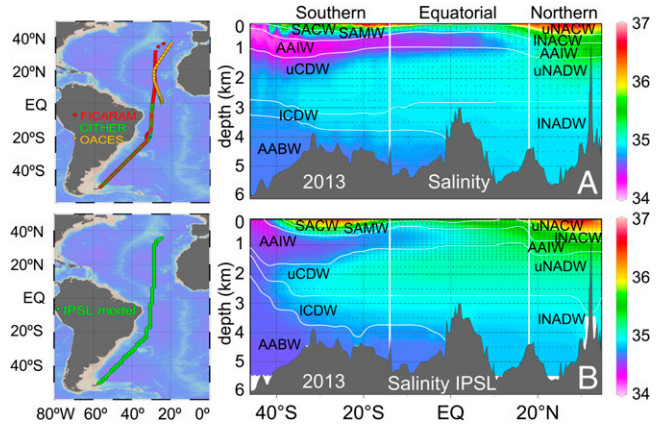

Fig. 1. (*A*, *Left*) Tracks of the OACES/CO_2 (1993), CITHER-II (1994), and FICARAM-XV (2013) cruises used in this study. (*Right*) The vertical distribution of salinity along the FICARAM-XV cruise in 2013. (*B*, *Left*) IPSL model profile. (*Right*) The vertical distribution of salinity of the model. The horizontal white lines are the selected isopycnals used to delimit the main water masses. For the model, the isopycnals were chosen according to their thermohaline characteristics (*SI Appendix*, Table S1). The vertical white lines divide the study area into three regions: southern (50°S–14°S), equatorial (14°S–18°N), and northern (18°N–36°N). Water mass acronyms: AABW, Antarctic Bottom Water; AAIW, Antarctic Intermediate Water; CDW, Circumpolar Deep Water; NACW, North Atlantic Central Water; NADW, North Atlantic Deep Water; SACW, South Atlantic Central Water; SAMW, Subantarctic Mode Water. The lowercase first letters "u" and "l" denote the "upper" and "lower" varieties of some of the water masses. Ocean Data View was used for mapping.

SI Appendix, Fig. S1). The highest pH values were found in South Atlantic Central Water (SACW) and upper North Atlantic Central Water (uNACW), with values up to 8.05 in the south and 7.9 in the north. The upper water values in the equatorial region were below 7.6. Along the southern region, the mixing of Antarctic Intermediate Water (AAIW), Subantarctic Mode Water (SAMW), and upper Circumpolar Deep Water (uCDW) in frontal zones led to intermediate pH values of ~7.7–7.6. The lowest pH values (<7.5) were in the AAIW layer of the equatorial region. The zonal circulation of the Equatorial Intermediate Current and the branches of the Northern South Equatorial Current and South Equatorial Countercurrent (19) were associated with pH minima. These pH minima were located in regions of high remineralization of organic matter, coinciding with oxygen minima centered at 13°S and 10°N (20). The Circumpolar Deep Water (CDW) and Antarctic Bottom Water (AABW) in the Southern Ocean were characterized by low pH values (~7.6).

Small but discernable changes in pH were observed over the two decades, especially in the layers above a depth of 2,000 m. These changes in pH (ΔpH), with negative values indicating a decrease in pH, were revealed by decreases throughout most of the water column (Fig. 2*B*). The greatest acidification was detected in the southern region from the surface to depths greater than 1,000 m. In this area, the average ΔpH reached −0.042 in the SACW, −0.037 in the SAMW, and −0.029 in the AAIW (Fig. 2*B* and Table 1). The northern region showed relatively strong acidification with average ΔpH values of −0.033 in the uNACW, −0.040 in the lower North Atlantic Central Water (lNACW), and −0.012 in the AAIW. Acidification was much weaker in the upper water column in the equatorial region. For example, ΔpH in the uCDW–uNADW layer was about two times higher in the southern and northern regions than in the equatorial region (−0.010 versus −0.005). Deeper in the water column, ΔpH values were similar along the transect, ranging from −0.006 to −0.007 in the lower Circumpolar Deep Water (lCDW)–lower North Atlantic Deep Water (lNADW) layer and up to −0.008 in the AABW layer.

The ΔpH was separated into changes associated with the increase in Cant in the ocean (ΔpHCant) and those associated with a modification in total inorganic carbon (C_T) resulting from the remineralization of organic matter and changes in ocean circulation (ΔpHNat). To separate the anthropogenic and natural components of ΔpH, a pH value (pH_{2013}-ant) was computed for 2013 from thermodynamic equations that included total alkalinity (A_T) and the nonanthropogenic changes in C_T (C_T − ΔCant). This computation yielded the anthropogenic C_T component of the pH change (ΔpHCant = pH_{2013} − pH_{2013}-ant), where pH_{2013} is the measured pH. The natural component (ΔpHNat) equaled ΔpH − ΔpHCant over the 20-y timespan. Cant concentrations were determined by the carbon-based φC_T^0 method (21, 22), with an SD in the changes in Cant (ΔCant) of ±2.7 μmol/kg. This SD translates into an uncertainty of 0.005 in ΔpHCant and ΔpHNat (*SI Appendix*, *SI Text*). To avoid biases in ΔpHNat caused by water mass mixing, the ΔpHNat was corrected for these effects using changes in potential temperature (Δθ) in the water masses from 1993 to 2013 (*SI Appendix*, Table S3).

Based on this analysis, the uptake of Cant by the ocean has been the main contributor to ΔpH over the last two decades (Table 1). As expected, ΔpHCant and ΔCant distributions showed similar patterns (Fig. 3 *A* and *D*), with the highest changes located in the upper layer in contact with the atmosphere. There is a clear south-to-north gradient, with ΔpHCant values in the southern region being about twice as large as in the equatorial and northern regions. In the surface layers, ΔpHCant reached values up to −0.039 in the southern region (SACW) and −0.030 in the equatorial and northern regions (SACW–uNACW), coinciding with the highest ΔCant values of 21 and 15 μmol/kg, respectively (Table 1). In the subsurface layer (SAMW–lNACW), ΔpHCant also showed higher absolute average values in the southern region (−0.033) than in the equatorial and northern regions (0.016), in agreement with the ΔCant values of 15 and 6 μmol/kg, respectively (Fig. 3 *A* and *D* and Table 1). Deeper in the ocean, ΔpHCant values dropped from around −0.018 (ΔCant ~7 μmol/kg) in the southern AAIW layer to between −0.003 and −0.010 (ΔCant ~1–4 μmol/kg) in the CDW and AABW layers. ΔpHCant and ΔCant were strongly correlated because ΔpHCant is caused directly by anthropogenic CO_2 entering the ocean and because ΔpHCant is computed from ΔCant (see above). Determining ΔCant by an independent method [transit time distribution (TTD)] in which no CO_2 measurements were used (23) yielded the same results (*SI Appendix*, Fig. S2).

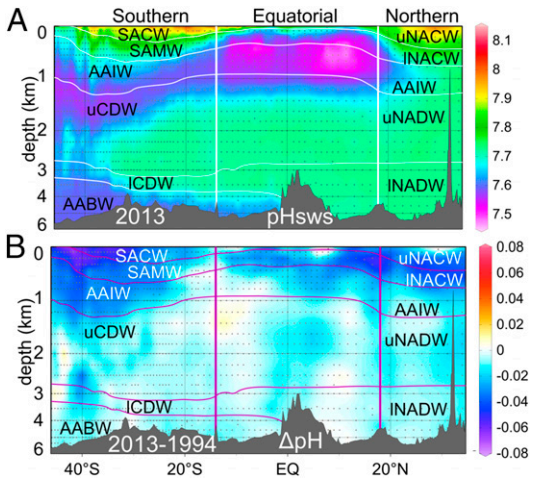

Fig. 2. Vertical distributions of (*A*) pH at 25 °C on the seawater scale (SWS) along 2013 and (*B*) pH_{SWS} changes (ΔpH) between 2013 and 1993–94. Ocean Data View was used for mapping. Note that the depth scale is not linear.

Table 1. Average values and SDs of each variable in each layer and region

Region	Layer	N	ΔpH·10³	ΔpHCant·10³	ΔpHNat·10³	ΔCant, μmol/kg	ΔCant-TTD, μmol/kg	ΔNO_3, μmol/kg	ΔpHCant-IPSL·10³	3.92xstd(pHNat) IPSL·10³
Southern	SACW	80	−42.1 ± 24.5	−38.8 ± 4.2	−5.5 ± 18.0	20.7 ± 2.6	19.2 ± 1.7	*-0.04 ± 1.21*	−34.2 ± 5.7	13.7 ± 5.0
50°S–14°S	SAMW	132	−36.5 ± 23.4	−33.2 ± 11.4	*-0.4 ± 20.9*	14.5 ± 5.5	13.9 ± 2.8	*-0.14 ± 1.41*	−32.5 ± 8.4	20.0 ± 5.5
	AAIW	230	−28.9 ± 13.9	−18.0 ± 9.4	−13.3 ± 13.1	6.8 ± 3.6	9.7 ± 3.3	0.32 ± 0.86	−12.2 ± 8.1	18.3 ± 11.5
	uCDW	401	−8.5 ± 13.7	−9.8 ± 6.7	*-0.1 ± 9.5*	3.8 ± 2.6	2.6 ± 1.2	−0.27 ± 0.77	0.3 ± 2.5	8.9 ± 7.1
	lCDW	48	−5.6 ± 13.3	−7.3 ± 6.6	5.2 ± 3.9	3.0 ± 2.6	1.9 ± 0.5	−0.53 ± 0.51	−2.0 ± 4.0	15.3 ± 7.5
	AABW	181	−7.9 ± 7.0	−7.7 ± 5.5	3.0 ± 3.8	2.9 ± 2.1	2.8 ± 0.6	−0.57 ± 0.65	−4.4 ± 6.4	17.7 ± 3.5
Equatorial	SACW	27	−19.7 ± 41.1	−30.0 ± 10.3	0.2 ± 30.8	14.7 ± 5.9	15.1 ± 2.7	0.54 ± 2.49	−27.6 ± 4.9	14.4 ± 7.2
14°S–18°N	SAMW	64	−24.2 ± 30.0	−16.2 ± 10.7	−9.2 ± 31.7	6.3 ± 4.2	8.5 ± 1.6	*0.30 ± 1.58*	−20.2 ± 2.2	12.7 ± 4.9
	AAIW	118	−13.6 ± 18.6	−3.8 ± 7.7	−12.2 ± 17.1	1.4 ± 2.7	3.6 ± 1.1	0.30 ± 0.96	−12.5 ± 3.0	6.6 ± 1.5
	uCDW	205	−4.7 ± 10.2	−3.0 ± 6.7	−1.9 ± 7.4	1.3 ± 2.7	1.7 ± 0.5	*0.04 ± 0.72*	−4.4 ± 2.5	5.1 ± 1.6
	lCDW	78	−4.4 ± 6.4	−3.0 ± 4.4	*-0.7 ± 5.2*	1.3 ± 1.8	1.3 ± 0.3	0.25 ± 0.56	−1.5 ± 3.0	6.3 ± 3.0
	AABW	41	−6.4 ± 6.2	−2.9 ± 6.4	*1.7 ± 6.7*	1.2 ± 2.5	1.4 ± 0.4	−0.28 ± 0.34	−9.0 ± 1.1	10.3 ± 1.0
Northern	uNACW	38	−33.3 ± 29.5	−30.6 ± 6.6	−13.4 ± 18.6	15.8 ± 4.4	16.9 ± 2.2	1.18 ± 1.73	−33.3 ± 7.3	19.1 ± 6.1
18°N–36°N	lNACW	23	−39.5 ± 21.8	−15.4 ± 8.1	−19.9 ± 18.5	6.4 ± 3.4	9.1 ± 3.1	1.03 ± 0.81	−19.3 ± 3.4	9.9 ± 3.0
	AAIW	35	−12.1 ± 13.8	−8.4 ± 7.0	−7.1 ± 12.0	3.4 ± 2.8	3.7 ± 2.1	*0.08 ± 0.70*	−13.9 ± 3.4	4.6 ± 1.2
	uNADW	63	−11.2 ± 8.9	−7.4 ± 6.4	−3.8 ± 7.0	3.1 ± 2.7	1.9 ± 1.3	*-0.02 ± 0.48*	−8.4 ± 3.8	5.3 ± 1.2
	lNADW	52	−6.9 ± 5.5	−3.4 ± 3.6	−3.6 ± 4.3	1.4 ± 1.5	1.0 ± 0.2	0.26 ± 0.33	0.0 ± 1.6	3.8 ± 1.9

Average values and SDs for each layer and region of pH change (ΔpH); the anthropogenic component of ΔpH (ΔpHCant); the natural component of ΔpH (ΔpHNat); the anthropogenic CO_2 change estimated by the φC_T^0 method (ΔCant) and by the TTD method (ΔCant-TTD); the change in nitrate (ΔNO_3) between 1993–94 and 2013 from observations; and ΔpHCant and ΔpHNat [= 3.92xstd(pHNat)] from the IPSL model. Italics indicate values that are not statistically significant (Student's *t* test <0.05). Column N indicates the number of values within each layer. See Fig. 1 for water mass acronyms.

ΔpHNat includes changes in pH related to changes in ocean circulation and/or biological activity, which are driven by natural variability and climate change. The pH changes associated with climate change were estimated to be less than 0.0001/y, i.e., <0.002 over the past two decades (9). We corrected ΔpHNat for mixing between the water masses by using the changes in potential temperature (Δθ) (*SI Appendix*, Table S3). ΔpHNat, therefore, primarily captured the natural interannual and decadal variability of the ocean's circulation and carbon cycle. This interannual-to-decadal variability was particularly pronounced in the higher latitudes of the North Atlantic (12, 24) and South Atlantic (25–28). ΔpHNat was generally lower than ΔpHCant, except in mode and intermediate waters (i.e., SAMW, lNACW, and AAIW), where ΔpHNat and ΔpHCant had similar magnitudes with rates up to −0.0010 ± 0.0002/y (Fig. 4*A* and Table 1). ΔpHNat patterns closely matched the patterns of changes in nitrate (ΔNO_3) corrected for mixing using Δθ (Fig. 3 *B* and *E*). The correlation coefficient (r^2) obtained between ΔpHNat and ΔNO_3 for all the water masses was 0.63, with a slope of −0.012 ± 0.002 and $P < 0.01$ (Fig. 4*B*). The relationship between ΔpHNat and ΔNO_3 is attributed to remineralization. The slope indicates that 0.012 units of pH change correspond to 1 μmol of NO_3. Thus a change of 0.001 units of pH is equivalent to 0.52 μmol of CO_2, from which a stoichiometric C:N ratio of 6.2, close to the Redfield ratio of 6.6, was obtained (29). Central and mode waters showed the largest changes in ΔpHNat (±0.030) and ΔNO_3 (±3 μmol/kg), findings that are in agreement with the spatial and temporal variability of the ocean's circulation and biology being stronger in the upper waters (Fig. 3 *B* and *E*). The intermediate water class with the largest change was the AAIW, with ΔpHNat up to −0.013 and ΔNO_3 up to 0.32 μmol/kg. The smallest changes occurred in the deep and bottom waters (±0.005 pH units and changes in NO_3 of ±0.5 μmol/kg) (Fig. 3 *B* and *E* and Table 1).

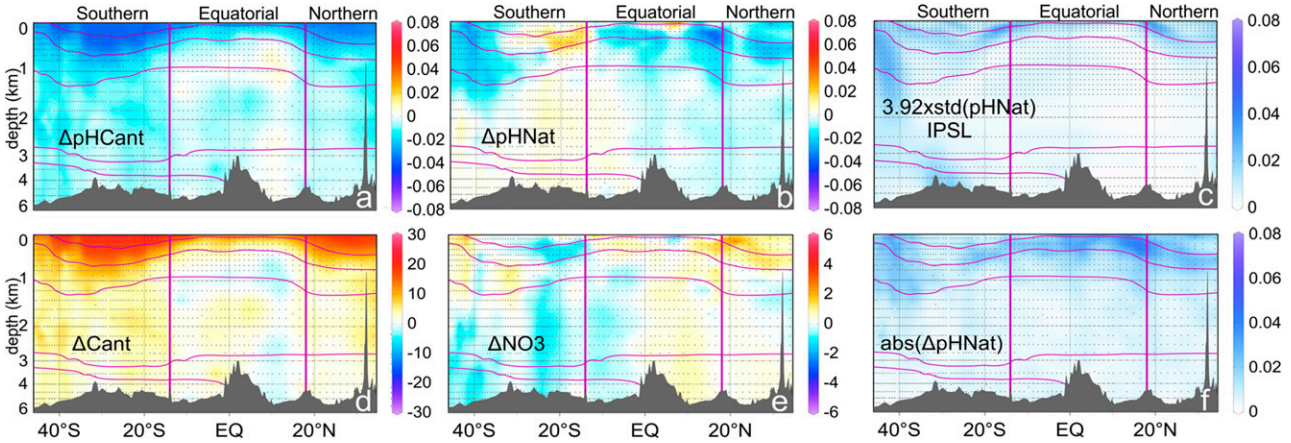

Fig. 3. Vertical distributions of changes between 1993/94 and 2013 in (*A*) the anthropogenic component of ΔpH (ΔpHCant), (*B*) the natural component of ΔpH (ΔpHNat), (*C*) ΔpHNat variability in the IPSL model [3.92 × std(pHNat)], (*D*) anthropogenic CO_2 (ΔCant) expressed in micromoles per kilogram, (*E*) nitrate (ΔNO_3) expressed in micromoles per kilogram, and (*F*) the absolute value in *B* [abs(ΔpHNat)] to show the magnitude of variability. Ocean Data View was used for mapping. Note that the depth scale is not linear.

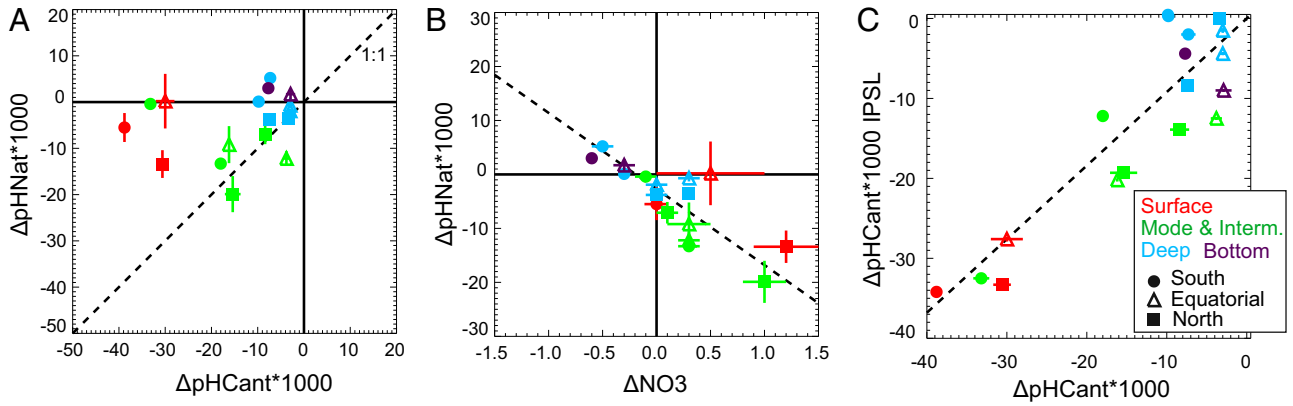

Fig. 4. (*A*) Observed ΔpHNat versus ΔpHCant, (*B*) Observed ΔpHNat versus ΔNO_3 (expressed in micromoles per kilogram) in the different layers of the three regions. ΔpHNat*1000 = −11.55 ± 2.26·ΔNO_3 = − 0.1 ± 1.1; r^2 = 0.63; $P < 0.01$. (*C*) ΔpHCant-PSL versus ΔpHCant-Observations. ΔpHCant = 0.92 ± 0.11·ΔpHCant-IPSL − 0.0009 ± 0.0019; r^2 = 0.83; $P < 0.01$. Error bars represent the SEM. Layers: Surface (SACW, uNACW), mode and intermediate (SAMW, lNACW, AAIW), deep (uCDW, uNADW, lCDW, lNADW), and bottom (AABW). (See Fig. 1 for water mass acronyms).

Discussion

The observed changes in pH in near-surface/upper waters were in general agreement with changes expected because of anthropogenic CO_2. However, there was an appreciable signal resulting from natural variability that was particularly pronounced in the intermediate waters and near-frontal systems. Surface layers showed acidification rates up to –0.0021 ± 0.0012/y in the South Atlantic, and high acidification rates also were observed in the water masses along the ventilation pathways, namely, mode waters with rates up to –0.0018 ± 0.0012/y in the South Atlantic and –0.0017 ± 0.0015/y in the North Atlantic. Intermediate waters showed changes up to –0.0014 ± 0.0007/y, whereas deep waters in the South Atlantic showed smaller changes of approximately –0.0004 ± 0.0003/y. Although, on average, acidification rates were higher in near-surface waters, the highest local values were observed in subsurface mode waters between the depths of 200 and 500 m. Higher acidification rates (i.e., more negative pH) in subsurface waters were in agreement with the high acidification rates observed in the subsurface waters at the ALOHA (A Long-term Oligotrophic Habitat Assessment) and BATS (Bermuda Atlantic Time-Series) time-series stations (12, 14) in the South Atlantic (30) and along a North Pacific section (7), respectively.

For the first time, to our knowledge, our observations confirm the major role of mode and intermediate waters (MW–IW) at the basin scale in the acidification of the ocean interior, which also was evidenced in the climate models (9). The high rates of acidification are attributed to the lower buffering capacity of mode waters compared with surface waters, because mode waters have a lower temperature and A_T/C_T ratio and therefore are more sensitive to increasing oceanic C_T (9, 10). In addition, mode waters have a larger exposure to the atmosphere, with a surface area-to-volume ratio five to 10 times larger than that of deeper waters, thus enabling a larger uptake of atmospheric CO_2 and, hence, stronger acidification (9).

The observed changes in pH in surface waters were largely of anthropogenic origin (Fig. 4*A*). The rates associated with anthropogenic forcing, ranging from –0.0015 to –0.0020/y, were found throughout the Atlantic surface waters from 50°S–36°N and are similar to rates previously reported in the South Atlantic (30) and by the European Station for Time Series in the Ocean in the North Atlantic (11). Modeling studies have confirmed the dominant role of atmospheric anthropogenic forcing on pH changes in the surface layers (2, 31). We found larger values of ΔpHCant, associated with larger ΔCant, in the South Atlantic than in the North Atlantic. The larger ΔCant in the south compared with the north is attributed partly to the southern transects of the cruises having been located in the western Atlantic, whereas the northern transects were located in the eastern Atlantic. Mode and deep water formation are concentrated in the western Atlantic in both hemispheres. Water masses in the northeastern region of the section are expected to be older than in the southwestern region and to have lower ΔCant values. However, another process probably explains why ΔCant and ΔpHCant were weaker in the North Atlantic. In the subpolar region of the North Atlantic, a weakening in the formation of Labrador Sea Water led to a decrease in the relative Cant inventory of North Atlantic Deep Water (NADW) from 1997 to 2003 (32) and to a smaller change in ΔpHCant. In contrast, a larger increase in the Cant inventory was found in the South Atlantic compared with the North Atlantic from 1989 to 2005 (33), possibly related to the Southern Annular Mode (SAM) affecting the uptake of Cant in the South Atlantic and to the North Atlantic Oscillation shift impacting ΔpHCant in the North Atlantic (34).

Our observations show that the anthropogenic and natural components had a similar magnitude in the MW–IW (Fig. 4*A*), indicating that changes in ocean circulation and biological activity contributed significantly to pH variability in the subsurface waters of the Atlantic Ocean over this time period. The observations were placed in the context of changes occurring in a larger space and time domain by comparing them with pH changes from the IPSL Earth System Model. This model objectively assessed the separation of ΔpH into ΔpHCant and ΔpHNat. The distribution of ΔpHCant in IPSL, referred to as "ΔpHCant-IPSL," followed the distribution obtained from the observations, with the largest changes in surface, mode, and intermediate waters associated with water mass ventilation and anthropogenic CO_2 uptake (Fig. 4*C*). The good correspondence between the model and the observations is reflected by a correlation between ΔpHCant-IPSL and ΔpHCant of 0.92 ± 0.11 and an intercept of –0.0009 ± 0.0019 (r^2 = 0.83, $P < 0.01$).

The IPSL simulations spanned the period from 1850 to 2014 and included the entire Atlantic Ocean, allowing the interannual-to-decadal variability of ΔpHNat determined during the 1993–94 and 2013 cruises to be placed in a larger context. Because climate models statistically represent the natural variability of the ocean–atmosphere system but not necessarily its exact timing (28), the variability patterns of ΔpHNat-IPSL are described in terms of the SD of the values along the cruise transect and are compared with the amplitude of the observed ΔpHNat [abs(ΔpHNat)] (Fig. 3 *C* and *F*). The comparison between the model and the observations therefore was not exact, because one is an SD over 164 y and the other is the difference between two sections over 20 y. The observed changes and

modeled ΔpHNat variability presented similar patterns, with large changes in the surface layers and in the MW–IW of the southern and northern regions (Fig. 3 *B* and *E*). The ΔpHNat in the equatorial region was smaller in the model than in the observations. However, the observed ΔpHNat was uncertain in surface, mode, and intermediate waters in the equatorial region, because these water masses are compressed into a thin layer of about 120 m with few measurements.

The model output was used to elucidate the controls of the large ΔpHNat in the MW–IW of the northern and southern regions. The observations showed a strong relationship between ΔpHNat and ΔNO_3 (Fig. 3 *B* and *E*) and between ΔpHNat and the apparent oxygen utilization (AOU) (*SI Appendix*, Fig. S3), which suggests that pHNat changes were mostly the result of changes in C_T from biological remineralization. The strong relationship between ΔpHNat and ΔNO_3 also was found in the MW–IW of the IPSL model, with 0.013 units of pH change per micromole of NO_3 ($r^2 = 0.93$). The model showed that 80% of the ΔpHNat could be explained by changes in C_T, whereas A_T accounted for 15–20% of the changes, and salinity accounted for less than 10% of the changes (Fig. 5*A*). For the pHNat variations attributed to C_T changes, 50–65% corresponded to the physical transport of C_T by ocean circulation, and 15–30% corresponded to in situ biological remineralization of organic matter within the water mass (Fig. 5*A*). The strong correlation between ΔpHNat and ΔNO_3 supports the notion that the increase in C_T controlled the observed pHNat changes but that transport of respired carbon was the main contributor, rather than local biological remineralization.

The largest observed and modeled pHNat changes in the MW–IW occurred where the water masses were formed and subjected to variability in surface forcing south of 40°S (Fig. 3 *C* and *F*). In the South Atlantic, the modeled ΔpHNat in newly formed water depended on the latitude where the formation occurred (Fig. 5*B*). Formation at higher latitudes led to the subduction of higher-C_T/lower-A_T waters, thereby decreasing ΔpHNat, with the opposite holding true if formation occurred at lower latitudes. In agreement with previous studies (35, 36), the model results suggest that the SAM might explain part of the latitudinal shift. The positive phase of the SAM shifts westerly winds and the MW–IW subduction poleward (Fig. 5*B*). Additionally, the positive phase of SAM increases the upwelling, northward Ekman transport, and subduction of C_T-enriched CDW into the MW–IW (37), thereby making ΔpHNat more negative. This mechanism was supported further by the higher AOU found in association with lower pHNat in both the observations (*SI Appendix*, Fig. S3) and the model (Fig. 5*B*). It explains the large observed decrease in pHNat in the MW–IW south of 40°S between 1993 and 2013 (Fig. 3*C*), because in this period the SAM trended positive.

In the North Atlantic, at the mode and intermediate outcrop, ΔpHNat variability in the model depended on the volume of newly formed water (Fig. 5*C*). When larger volumes of MW–IW were formed, a larger proportion of the deeper CO_2- and AOU-rich waters of northern origin were subducted (*SI Appendix*, Fig. S4), leading to more negative ΔpHNat. There is observational evidence that the winter-mixed layer depth (38), volume, and AOU content (39) of the MW–IW in the North Atlantic have increased over the past decades. This mechanism could explain the decrease in pHNat observed in the MW–IW in the North Atlantic between 1993 and 2013.

In summary, the observations and model show that decreases in the pH of near-surface waters are dominated by the contribution of Cant. In the MW–IW, anthropogenic and natural components are of the same order of magnitude and are in the same direction from 1993 to 2013, with natural changes reinforcing the anthropogenic acidification signal. The observations and model output confirm that, although carbonate chemistry and geochemical properties of the water masses are crucial for explaining long-term changes in pH and oxygen levels (3, 9), changes in ocean circulation and biological production (13, 14, 40) also exert a large impact on pH on interannual-to-decadal time scales in subsurface waters. Based on projections of future increases in atmospheric CO_2 and the associated penetration of Cant into intermediate and deep waters, the contribution of anthropogenic forcing to the acidification of subsurface waters will increase with time and eventually will exceed natural variability and trends.

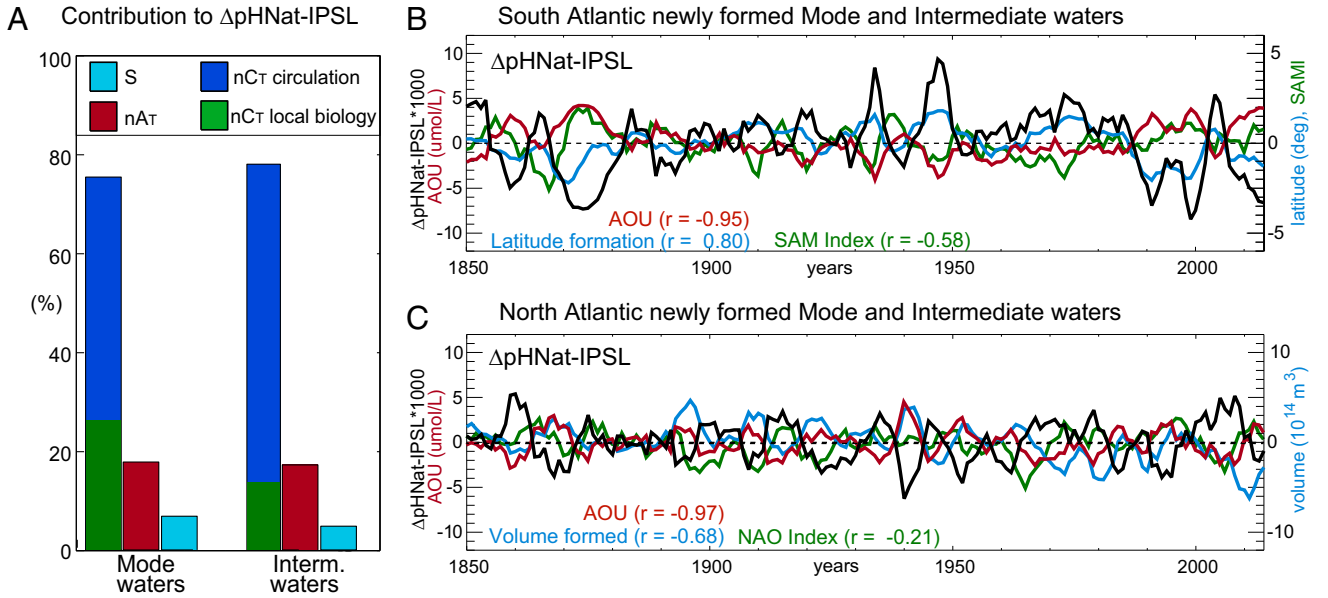

Fig. 5. ΔpHNat in mode and intermediate waters (MW–IW) over the Atlantic Ocean (80°S–65°N) in the IPSL model. (*A*) Contribution to ΔpHNat associated with changes in salinity (S, cyan), changes in normalized A_T (nA_T, red), and changes in normalized C_T (nC_T) caused by physical transport (blue) and biological activity (green). (*B* and *C*) ΔpHNat time-series in newly formed MW–IW in the South Atlantic (*B*) and North Atlantic (*C*). Anomalies in latitude, volume of formed waters, AOU, SAM index, and North Atlantic Oscillation (NAO) index also are shown with their correlation coefficient to ΔpHNat.

Materials and Methods

Data Processing. To obtain the changes in the variables (pH, Cant, Cant-TTD, θ, and NO_3) between 1993–94 and 2013, we used the position and depth of the 100 stations of the FICARAM-XV line as a base. Data from the 94 stations of CITHER-II and the 42 stations of OACES/CO_2 that coincided with the FICARAM-XV line were interpolated to the station positions and depths of FICARAM-XV using a Delaunay triangulation to obtain an interpolated dataset with the same grid for both periods. This interpolated dataset allowed us to determine differences in the variables over the 20-y time period. For Table 1, we determined an average and SD for all of the values in a particular water mass ("layer") for each region. More details on the datasets can be found in *SI Appendix*, Table S1.

Uncertainties. The uncertainty of ΔpH amounted to 0.0035 based on the analytical uncertainty of each pH dataset (0.001, 0.003, and 0.0015 for OACES/CO_2, CITHER-II, and FICARAM-XV, respectively). The uncertainty of Cant was based on a propagation of error for each of the variables used in the calculation that yielded an SD of ΔCant of 2.7 μmol/kg. This calculation translates to an uncertainty of 0.005 in ΔpHCant and ΔpHNat, which is the maximum error for ΔpHCant as shown in *SI Appendix, SI Text*.

The IPSL Climate Model. The low-resolution (LR) IPSL climate model (IPSL-CM5A-LR), which participated in the Coupled Model Intercomparison Project Phase 5 (10) was used. The IPSL simulations covered the period from 1850 to 2014. They included sensitivity experiments separating anthropogenic perturbations from natural variability and climate-induced feedbacks. Four IPSL simulations were investigated: (*i*) the historical run from 1850 to 2005, with increasing CO_2 concentrations and changes in radiative forcing such as volcanoes and aerosols; (*ii*) an "intermediate" representative concentration pathway (RCP4.5) for the period 2006–2014, characterized by an additional radiative forcing of 4.5 W/m^2 and corresponding to a CO_2 atmospheric concentration of 538 ppm in 2100; (*iii*) a sensitivity experiment (esmFdbk2) from 1850 to 2014 that included the increased radiative forcing of scenario RCP4.5 but with no increase in atmospheric CO_2 (this scenario represents climate change and variability without Cant entering the ocean and corresponding to ΔpHCant); and (*iv*) a control simulation (piControl) from 1850 to 2014 that included only internal variability in the model with no changes in forcing or atmospheric CO_2. This simulation was used to correct for possible model drift. The esmFdbk2 simulation was used to isolate pHNat, that is, the contribution of natural variability and climate change feedbacks, such as changes in ocean circulation and biological activity, from the chemical effects of increasing CO_2 concentration. Once the pHNat contribution was removed from the historical run, ΔpHCant-IPSL was computed from the difference between 2013 and 1993.5 at the 111 profiles of the FICARAM-XV section using the model pixel closest to the station location (Fig. 1*B*). The ΔpHNat-IPSL was estimated using the interannual anomaly of pHNat over the 164 y of the simulation, and std(ΔpHNat-IPSL) was based on the 95% confidence interval of ΔpHNat-IPSL ($\pm 1.96 \times$ SD, i.e., $3.92 \times$ SD). Although the model results were compared with observations along the cruise transect (Fig. 1*B*), the processes regulating ΔpHNat in the MW–IW were computed for the entire Atlantic basin (80°S–65°N). The SAM index was computed based on sea-level pressure.

ACKNOWLEDGMENTS. We thank the officers and crews of the National Oceanographic and Atmospheric Administration (NOAA) ship *Malcolm Baldrige*, Research Vessel (R/V) *Maurice Ewing*, and R/V *Hespérides*, along with the scientific and technical teams, for their support during the OACES/CO_2, CITHER-II, and FICARAM-XV cruises; Gail Derr of the Atlantic Oceanographic and Meteorological Laboratory of the NOAA for copyediting the manuscript; and the editor and two anonymous reviewers for their critical reading and constructive comments. This research was supported by the Spanish Ministry of Sciences and Innovation and was cofunded by the European Regional Development Fund 2007–2012 (FEDER) through the Carbon Transport and Acidification Rates in the North Atlantic Project (CTM2010-17141/MAR), by the European Union Seventh Framework Programme CARBOCHANGE project under Grant Agreement 264879, and by the Office of Atmospheric and Oceanic Research of the NOAA.

1. Caldeira K, Wickett ME (2003) Oceanography: Anthropogenic carbon and ocean pH. *Nature* 425(6956):365.
2. Orr JC, et al. (2005) Anthropogenic ocean acidification over the twenty-first century and its impact on calcifying organisms. *Nature* 437(7059):681–686.
3. Orr JC (2011) Recent and future changes in ocean carbonate chemistry. *Ocean Acidification*, eds Gatuso JP, Hansson L (Oxford Univ Press, Oxford, UK), pp 41–66.
4. Feely RA, et al. (2004) Impact of anthropogenic CO_2 on the $CaCO_3$ system in the oceans. *Science* 305(5682):362–366.
5. Doney SC, Fabry VJ, Feely RA, Kleypas JA (2009) Ocean acidification: The other CO_2 problem. *Annu Rev Mar Sci* 1:169–192.
6. Hofmann GE, et al. (2010) The effects of ocean acidification on calcifying organisms in marine ecosystems: An organism to ecosystem perspective. *Annu Rev Ecol Evol Syst* 41:127–147.
7. Byrne RH, Mecking S, Feely RA, Liu X (2010) Direct observations of basin-wide acidification of the North Pacific Ocean. *Geophys Res Lett* 37:L02601.
8. Vázquez-Rodríguez M, Pérez FF, Velo A, Ríos AF, Mercier M (2012) Observed trends of anthropogenic acidification in North Atlantic water masses. *Biogeosciences* 9:5217–5230.
9. Resplandy L, Bopp L, Orr JC, Dunne JP (2013) Role of mode and intermediate waters in future ocean acidification: Analysis of CMIP5 models. *Geophys Res Lett* 40:1–5.
10. Olafsson J, et al. (2009) Rate of Iceland Sea acidification from time series measurements. *Biogeosciences* 6:2661–2668.
11. González-Dávila M, Santana-Casiano JM, Rueda M-J, Llinás O (2010) The water column distribution of carbonate system variables at the ESTOC site from 1995 to 2004. *Biogeosciences* 7:3067–3081.
12. Bates NR, et al. (2012) Detecting anthropogenic carbon dioxide uptake and ocean acidification in the North Atlantic Ocean. *Biogeosciences* 9:2509–2522.
13. Wakita M, et al. (2013) Ocean acidification from 1997 to 2011 in the subarctic western North Pacific Ocean. *Biogeosciences* 10:7817–7827.
14. Dore JE, Lukas R, Sadler DW, Church MJ, Karl DM (2009) Physical and biogeochemical modulation of ocean acidification in the central North Pacific. *Proc Natl Acad Sci USA* 106(30):12235–12240.
15. Lauvset SK, Gruber N, Landschützer P, Olsen A, Tjiputra J (2015) Trends and drivers in global surface ocean pH over the past three decades. *Biogeosciences* 12:1285–1298.
16. Ríos AF, Velo A, Pardo PC, Hoppema M, Pérez FF (2012) An update of anthropogenic CO_2 storage rates in the western South Atlantic basin and the role of Antarctic Bottom Water. *J Mar Syst* 94:197–203.
17. Talley LD, Pickard GL, Emery WJ, Swift JH (2011) Atlantic Ocean. *Descriptive Physical Oceanography: An Introduction*, eds Talley LD, Pickard GL, Emery WJ, Swift JH (Academic, Boston), pp 245–301.
18. Mémery L, et al. (2000) The water masses along the western boundary of the south and equatorial Atlantic. *Prog Oceanogr* 47:69–98.
19. Stramma L, England M (1999) On the water masses and main circulation of the South Atlantic Ocean. *J Geophys Res* 104(C9):20863–20883.
20. Wienders N, Arhan M, Mercier H (2000) Circulation at the western boundary of the South and Equatorial Atlantic: Exchanges with the ocean interior. *J Mar Res* 58:1007–1039.
21. Vázquez-Rodríguez M, et al. (2009) Anthropogenic carbon distributions in the Atlantic Ocean: Data-based estimates from the Arctic to the Antarctic. *Biogeosciences* 6:4527–4571.
22. Vázquez-Rodríguez M, Padín XA, Ríos AF, Pérez FF (2012) The subsurface layer memory of water mass formation conditions in the Atlantic: A reliable reference to estimate preformed properties and air-sea CO_2 disequilibria. *J Mar Syst* 92:52–63.
23. Waugh D, Hall TM, McNeil BI, Key R, Matear RJ (2006) Anthropogenic CO_2 in the oceans estimated using transit time distributions. *Tellus B Chem Phys Meterol* 58:376–389.
24. Keller K, et al. (2012) Variability of the ocean carbon cycle in response to the North Atlantic Oscillation. *Tellus B Chem Phys Meterol* 64:18738.
25. Lenton A, Matear RJ (2007) Role of the Southern Annular Mode (SAM) in Southern Ocean CO_2 uptake. *Global Biogeochem Cycles* 21:GB2016.
26. Lovenduski NS, Gruber N, Doney SC (2008) Toward a mechanistic understanding of the decadal trends in the Southern Ocean carbon sink. *Global Biogeochem Cycles* 22:GB3016.
27. Dufour CO, et al. (2013) Eddy compensation and controls of the enhanced sea-to-air CO_2 flux during positive phases of the Southern Annular Mode. *Global Biogeochem Cycles* 27:950–961.
28. Levine NM, Doney SC, Wanninkhof R, Lindsay K, Fung IY (2008) The impact of ocean carbon system variability on the detection of temporal increases in anthropogenic CO_2. *J Geophys Res* 113:C03019.
29. Redfield AC, Ketchum BH, Richard FA (1963) The influence of organisms on the composition of sea-water. *The Sea*, ed Hill MN (J Wiley and Sons, New York), Vol 2, pp 26–77.
30. Salt LA, van Heuven SMAC, Claus ME, Jones EM, de Baar HJW (2015) Rapid acidification of mode and intermediate waters in the southwest Atlantic Ocean. *Biogeosciences* 12:1387–1401.
31. Friedrich T, et al. (2012) Detecting regional anthropogenic trends in ocean acidification against natural variability. *Nat Clim Chang* 2:167–171.
32. Steinfeldt R, Rhein M, Bullister JL, Tanhua T (2009) Inventory changes in anthropogenic carbon from 1997–2003 in the Atlantic Ocean between 20°S and 65°N. *Global Biogeochem Cycles* 23:GB3010.
33. Wanninkhof R, et al. (2010) Detecting anthropogenic CO_2 changes in the interior Atlantic Ocean between 1989 and 2005. *J Geophys Res* 115:C11028.
34. Levine NM, et al. (2011) The impact of the North Atlantic Oscillation on the uptake and accumulation of anthropogenic CO_2 by North Atlantic Ocean mode waters. *Global Biogeochem Cycles* 25:GB3022.
35. Oke PR, England MH (2004) Oceanic response to changes in the latitude of the Southern Hemisphere subpolar westerly winds. *J Clim* 17:1040–1054.
36. Saenko OA, Fyfe JC, England MH (2005) On the response of the oceanic wind-driven circulation to atmospheric CO_2 increase. *Clim Dyn* 25:415–416.
37. Ayers JM, Strutton PG (2013) Nutrient variability in Subantarctic Mode Waters forced by the SAM and ENSO. *Geophys Res Lett* 40:3419–3423.
38. Carton JA, Grodsky SA, Liu H (2008) Variability of the oceanic mixed layer, 1960–2004. *J Clim* 21:1029–1047.
39. Stendardo I, Kieke D, Rhein M, Gruber N, Steinfeldt R (2015) Interannual to decadal oxygen variability in the mid-depth water masses of the eastern North Atlantic. *Deep Sea Res Part I Oceanogr Res Pap* 95:85–98.
40. Deutsch C, Emerson S, Thompson L (2006) Physical-biological interactions in North Pacific oxygen variability. *J Geophys Res* 111:C09S90.